

Novel Peptide-Calix[4]arene Conjugate Inhibits $A\beta$ Aggregation and Rescues Neurons from $A\beta$'s Oligomers Cytotoxicity *In Vitro*

Grazia Maria Letizia Consoli,* Rita Tosto, Ausilia Baglieri, Salvatore Petralia, Tiziana Campagna, Giuseppe Di Natale, Stefania Zimbone, Maria Laura Giuffrida, and Giuseppe Pappalardo*

Cite This: *ACS Chem. Neurosci.* 2021, 12, 1449–1462

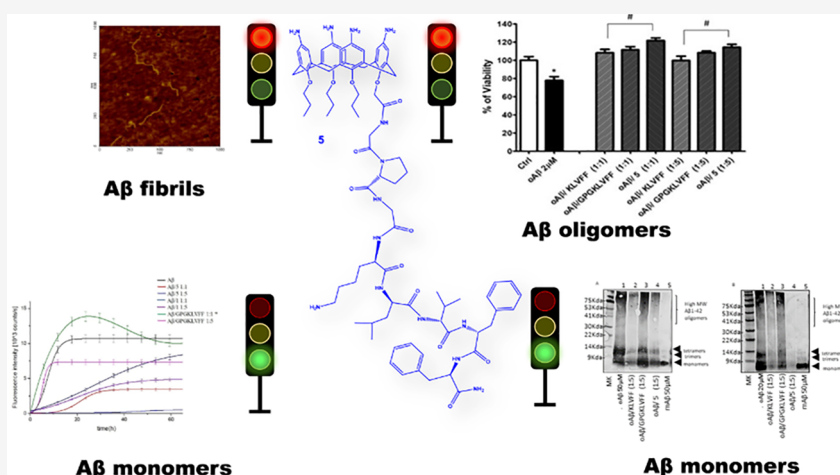
Read Online

ACCESS |

Metrics & More

Article Recommendations

Supporting Information



ABSTRACT: Alzheimer's disease (AD) is a progressive neurodegenerative condition affecting people in the elderly. Targeting aggregation of β -amyloid peptides ($A\beta$) is considered a promising approach for the therapeutic treatment of the disease. Peptide based inhibitors of β -amyloid fibrillation are emerging as safe drug candidates as well as interesting compounds for early diagnosis of AD. Peptide conjugation via covalent bond with functional moieties enables the resultant hybrid system to acquire desired functions. Here we report the synthesis, the structural characterization, and the $A\beta_{42}$ interaction of a *p*-amino-calix[4]arene derivative bearing a GPGKLVFF peptide pendant at the lower rim. We demonstrate that the *p*-amino-calix[4]arene-GPGKLVFF conjugate alters the $A\beta_{42}$ aggregation pathways by preventing $A\beta_{42}$'s conformational transition from random coil to β -sheet with concomitant changes of the aggregation kinetic profile as evidenced by circular dichroism (CD), thioflavin T (ThT), and dynamic light scattering (DLS) measurements, respectively. High resolution mass spectrometry (HR-MS) confirmed a direct interaction of the *p*-amino-calix[4]arene-GPGKLVFF conjugate with $A\beta_{42}$ monomer which provided insight into a possible working mechanism, whereas the alteration of the $A\beta_{42}$'s fibrillary architecture, by the calix-peptide conjugate, was further validated by atomic force microscopy (AFM) imaging. Finally, the herein proposed compound was shown to be effective against $A\beta_{42}$ oligomers' toxicity in differentiated neuroblastoma cells, SH-SY5Y.

KEYWORDS: $A\beta$ oligomers, amyloid, calixarenes, peptides, SH-SY5Y cells

INTRODUCTION

Alzheimer's disease (AD) is associated with a progressively neurodegenerative condition leading to dementia that mostly affects older people. AD represents one of the "protein misfolding diseases" with the highest socioeconomic impact¹ and still denotes a serious threat and an important challenge for scientific research in both the therapeutic and diagnostic fields. The cause and progression of the disease are not yet fully elucidated, being AD, especially the sporadic, late onset form of the disease (LOAD), linked to genetic or environmental risk factors, many of which are not still completely

clarified.² Currently, the therapeutic treatments, available in the market, offer only small symptomatic benefits and in part can slow down the course of the disease. One of the pathological hallmarks of AD is the presence of extracellular

Received: March 3, 2021

Accepted: March 30, 2021

Published: April 12, 2021



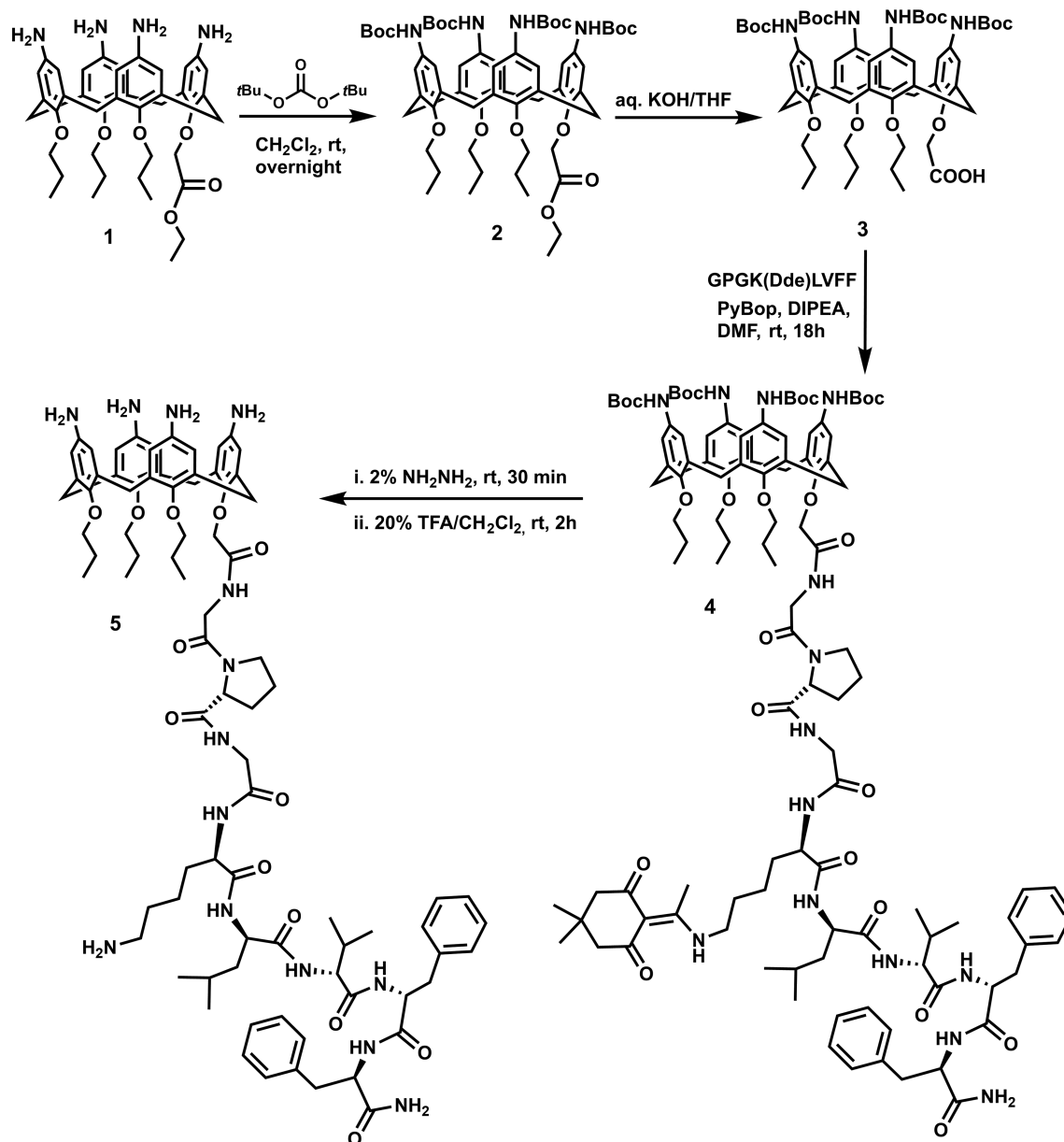
plaques mainly composed of aggregated forms of amyloid- β ($A\beta$) peptide, a 39–43 residue fragment derived from the amyloid precursor protein (APP).³ Recent studies demonstrate that early stage prefibrillar aggregates such as oligomers and protofibrils are highly toxic species in the central nervous system compared to mature fibrils.^{4,5} Structural information about the toxic oligomeric $A\beta$ species underlying AD has been difficult to obtain at an atomic level.⁶ The transient and heterogeneous properties of these assemblies imposes many challenges for the understanding of the multiple toxic mechanisms. Some oligomers are proposed to impart their toxic function by interacting directly with the cell membrane of neurons with consequent permeabilization and disruption.^{7,8} Thus, unveiling the structural features of oligomeric $A\beta$ species is turning a topical field of investigation propaedeutic for the design of effective therapeutics that target these pathogenic $A\beta$ species.^{9,10} $A\beta_{42}$ aggregates into 6–10 nm diameter fibrils with the characteristic cross- β structure.³ Preventing $A\beta_{42}$ peptide aggregation is therapeutically attractive, since $A\beta$ aggregation is an exclusively pathological process.¹¹ Selective targeting of $A\beta$'s fibrillogenesis should not interfere with the physiological function of APP as well as other proteins involved in the production of $A\beta$ monomers, whose physiological beneficial role has been recently reported.¹² Several small molecules, metal chelators, carbohydrate-containing compounds, and short peptides have been identified as inhibitors of amyloid aggregation.^{13–16} In particular, the clinical evidence of an abnormal metal ion interaction with $A\beta$ in AD has promoted studies aimed at developing potential therapeutic strategies by using metal chelators or antioxidant compounds that target aberrant metal distribution and the adverse consequences of metal induced oxidative stress in AD.^{17–19} The finding that the hydrophobic core at residues 16–20 of $A\beta$ (KLVFF) is crucial for the formation of β -sheet structures²⁰ has stimulated the investigation of the KLVFF peptide as an inhibitor of $A\beta_{42}$ fibrillogenesis.²¹ Some papers in the past reported that the KLVFF peptide, by binding the homologous sequence in full-length $A\beta$, can prevent at aggregation into fibrils^{13,22,23} and this ability is maintained after conjugation to different scaffolds including oligolysines,²⁴ cyclodextrins,²⁵ dendrimers,²⁶ or porphyrins.^{27,28}

Therefore, conjugation has emerged as a popular mechanism to modify or enhance the properties of a peptide drug candidate.^{29,30} Conjugation can also be used to deliver a cytotoxic payload or imaging agent to specific cell types targeted by the peptide.³¹ Calix[n]arenes are macrocyclic polyphenols proposed as molecular scaffolds for different fields of application.³² These macrocycles due to the peculiar structure and synthetic versatility have gained great interest in supramolecular chemistry. The calix[4–8]arene oligomers possess a hydrophobic cavity able to host a variety of guests and can cluster and spatially organize multiple ligands, providing rigid or flexible constructs suited for molecular recognition events. The low toxicity and immunogenicity exhibited by a variety of calix[n]arene derivatives have advanced these macrocycles to applications in biomedical and pharmaceutical fields.³³ Calix[n]arene derivatives have been proposed as anticancer,³⁴ antibacterial,³⁵ synthetic vaccines,³⁶ imaging agents,³⁷ and drug³⁸ and gene³⁹ delivery systems. Opportunely functionalized, the calix[n]arenes have also been exploited as biomimetic models to better understand relevant biological processes underlying the protein–protein or protein–carbohydrate interactions.⁴⁰ Yet, calix[n]arenes have

been successfully used as novel compounds for protein detection⁴⁰ and protein modulation.⁴¹ However, despite the wide use of calix[n]arenes in several fields of application, very few papers have dealt with the interactions of calix[n]arene derivatives with $A\beta$. Wang et al. described *p*-sulfonate-calix[4,6,8]arenes with anti- and disaggregating effect on $A\beta_{42}$ through nonspecific hydrophobic interactions.⁴² Guo et al. synthesized a nanoassembly consisting of multiple units of a *p*-sulfonate calix[4]arene and a β -cyclodextrin, which by means of the multiple complexing cavities exposed on the nanoassembly surface bind $A\beta_{42}$, inhibiting its aggregation or inducing fibril disaggregation.⁴³ We determined that endowing the calixarene macrocycle with an $A\beta$ recognition motif would generate a more refined tool to contrast the detrimental effects of the aggregated forms of $A\beta$ peptides. Thus, we resorted to the design and synthesis of a new calix[4]arene–peptide conjugate composed of a *p*-amino-calix[4]arene derivative bearing a GPGKLVFF peptide sequence at the macrocycle lower rim. We describe herein the synthesis and structural characterization of this hybrid system, alongside its capability to hamper $A\beta_{42}$ aggregation *in vitro*. The study has been carried out using a variety of spectroscopic techniques including circular dichroism (CD), thioflavin T (ThT) fluorescence, dynamic light scattering (DLS), and atomic force microscopy (AFM) imaging. High resolution mass spectrometry (HR-MS) was employed to point out direct interaction of the *p*-amino-calix[4]arene-GPGKLVFF conjugate with the $A\beta_{42}$ monomer. We also aim at providing *in vitro* experimental evidence of the ability of this novel construct to prevent the $A\beta$ oligomer cytotoxic effects on differentiated SH-SY5Y neuronal cultures. We demonstrate that the calix–peptide conjugate is *per se* nontoxic to neuronal cells and this allows its potential use as therapeutic agent in AD.

RESULTS AND DISCUSSION

Design and Synthesis of Calix[4]arene–GPGKLVFF (5). In search of functional calix[n]arene inhibitors of $A\beta$ amyloid fibrillogenesis, we thought that joining an $A\beta$ recognition peptide moiety to the framework of a water-soluble *p*-amino-calix[4]arene derivative would result in a new hybrid construct able to efficiently interact with $A\beta$ peptides and therefore hampering peptide chain's self-assembly into oligomeric/fibrillary toxic species. We chose the GPGKLVFF sequence because of the established ability of the KLVFF motif to recognize the homologous region of the parent full-length $A\beta$ peptide. The additional GPG tripeptide was inserted to reduce any eventual propensity to self-aggregation of the calix–peptide conjugate. The *p*-amino-calix[4]arene scaffold should confer enhanced water solubility to the resultant calix–peptide conjugate, at the same time establishing multiple noncovalent contacts with the aromatic and anionic amino acid residues of the $A\beta$ peptide. Moreover, it is expected that the calix–peptide conjugate would generate a steric hindrance between adjacent peptide chains thereby disturbing the $A\beta$'s self-assembly process. Compared to other peptide-conjugated systems, the peptide–calixarene difunctional compound can offer some advantages deriving from the known complexing properties of the calixarene cavity, in addition to the anti-amyloidogenic action of β -sheet breaker pentapeptide KLVFF as a “binding element” for targeting $A\beta$. The calixarene moiety might also synergically assist the peptide ligand in both $A\beta$ monomer stabilization and protection of neurons from $A\beta$ oligomeric insult. The calix–peptide hybrid system might in

Scheme 1. Synthetic Route for the Preparation of the *p*-Amino-calix[4]arene–GPGKLVFF Conjugate (5)

principle be useful for delivery purposes of AD active compounds or imaging agents for theragnostic application.

The procedure for the preparation of the calix-peptide conjugate (**5**) starting from compound **1**⁴⁴ is depicted in Scheme 1. In brief, for the preparation of compound **1**⁴⁴ the starting material *p*-*tert*-butyl-calix[4]arene was blocked in a cone conformation by tetra-functionalization of its lower rim with three propyl groups and one ethyl acetate group. Amino groups were introduced at the calix[4]arene upper rim, by ipso-nitration followed by C/Pd catalyzed reduction of the nitro groups. Before the coupling reaction with the peptide fragment, the amino groups at the upper rim were protected by *tert*-butyloxycarbonyl (Boc) groups to give compound **2**. Hydrolysis reaction provided compound **3** in which the COOH group at the lower rim can be used for the linkage of the GPGK(Dde)LVFF pendant via amide bond (Dde: N-(1-(4,4-dimethyl-2,6-dioxocyclohexylidene)ethyl). The GPGK-(Dde)LVFF sequence was synthesized by using the standard

microwave assisted Solid Phase Peptide Synthesis (mw-SPPS) reported in the literature,⁴⁵ and characterized by HR-ESI-MS (see Figure S1 Supporting Information). Peptide conjugation to the calix[4]arene scaffold was accomplished in solution and in the presence of PyBop as a condensing agent. The selective removal of the Dde and Boc protecting groups, by sequential treatment with hydrazine and trifluoroacetic acid respectively, gave the compound **5** whose molecular identity was confirmed by combined MALDI-TOF-MS, HR-ESI-MS and 1D/2D NMR spectra (Supporting Information Figures S2–S10).

Calix[4]arene–GPGKLVFF (5)/ $A\beta_{42}$ Interactions. To assess the inhibitory properties of **5** toward $A\beta_{42}$ fibril formation, we carried out a combined CD and ThT fluorescence study. DLS and AFM measurements aided the determination of the size and morphology of the $A\beta_{42}$ aggregates, respectively.

CD Spectroscopy. The conformational transition from a random coil to a β -sheet structure is the crucial step for the

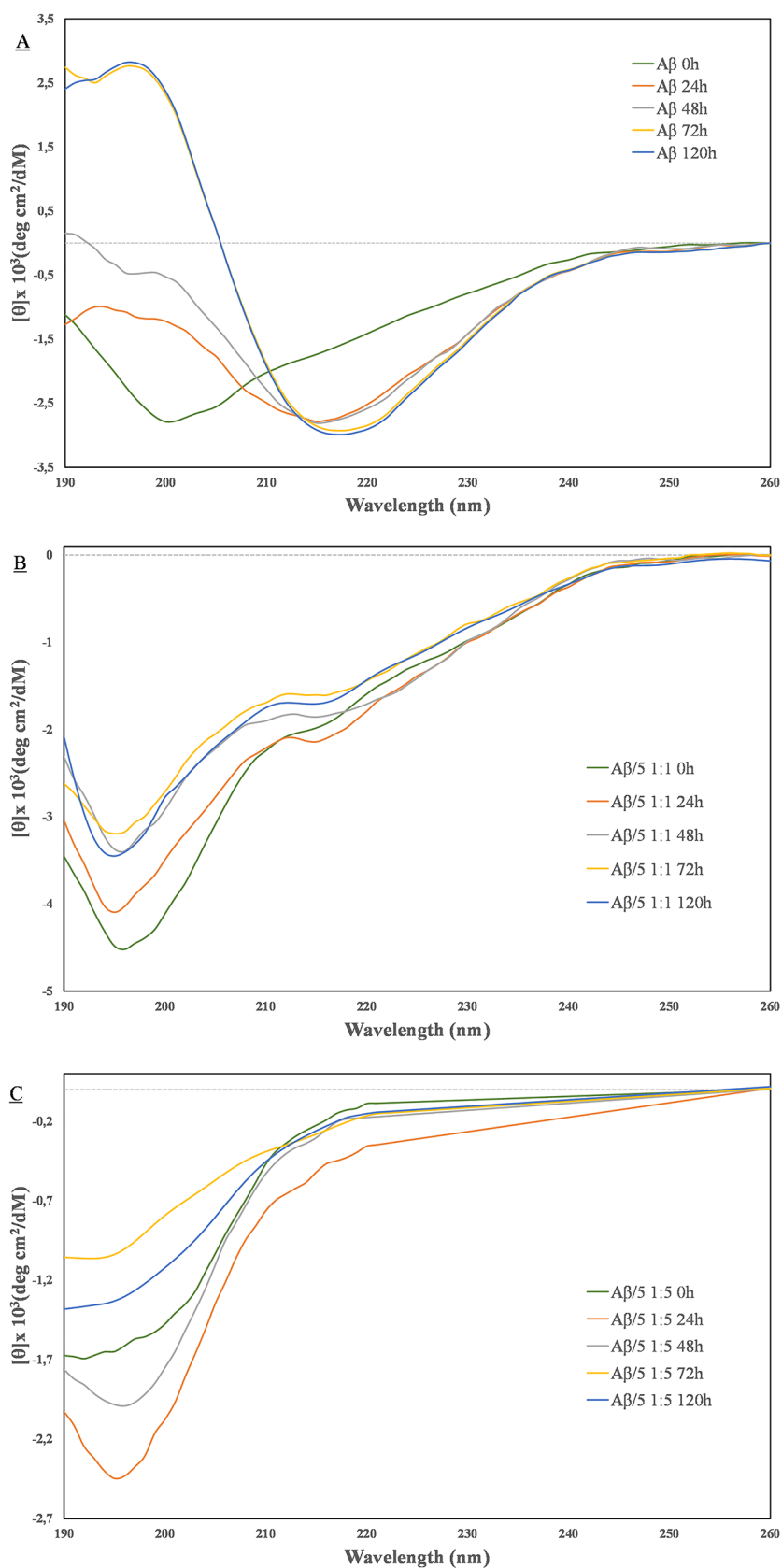


Figure 1. CD spectra of (A) $A\beta_{42}$, (B) $A\beta_{42}/5$ (1:1 molar ratio), and (C) $A\beta_{42}/5$ (1:5 molar ratio) recorded at different times.

fibrillogenesis of $A\beta_{42}$.⁴⁶ A series of time course CD experiments, either with pure $A\beta_{42}$ samples or $A\beta_{42}$

coincubated with compounds **1** or **5** in phosphate buffer (10 mM, pH 7.4), were carried out to examine the effect of these

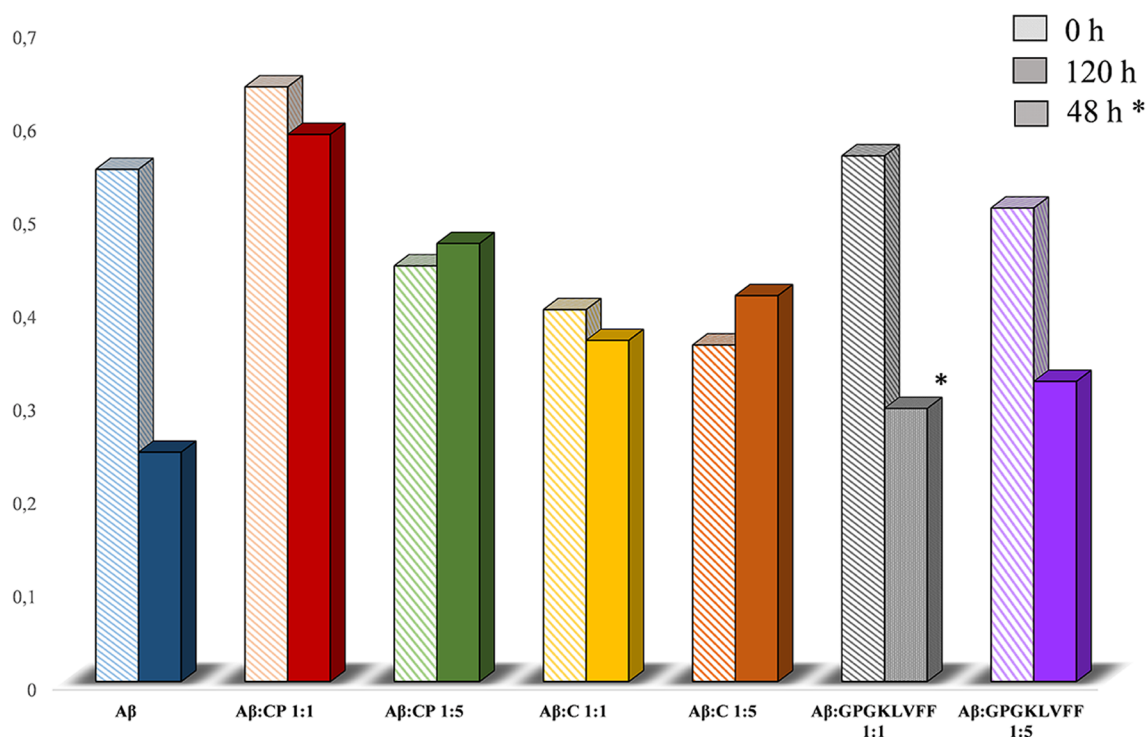


Figure 2. Graphical representation of the average percentage of unordered peptide conformation as determined by using CONTIN and CDSSTR deconvolution algorithms. CP = conjugate 5; C = compound 1. *Refers to 48 h incubation because of massive sample precipitation.

derivatives on the $A\beta_{42}$'s β -sheet conformational transition. Figure 1 shows the CD spectra recorded for $A\beta_{42}$ alone and in the presence of compound 5. It is clear from Figure 1 that, in the absence of 5, the $A\beta_{42}$ sample ($5 \mu\text{M}$) undergoes to an almost complete β -sheet conformational transition after 72 h. In fact, the freshly prepared $A\beta_{42}$ sample displays clear negative dichroism below 200 nm that is typical of a randomly coiled peptide chain. This curve profile gradually changes toward the β -sheet pattern, as the incubation time proceeds. The CD spectrum recorded at 72 h incubation time shows positive ellipticity at 190 nm along with a negative signal at 218 nm, thereby indicating the presence of β -sheet peptide structures.⁴⁷ This pattern does not change significantly after this time, indicating that $A\beta_{42}$ almost reaches the final state after 5 days of incubation. The CD spectra recorded in the presence of 5, either at equimolar or 5 mol excess, never display the characteristic β -sheet pattern. More interestingly, the observed CD spectra recorded at 5-fold molar excess always exhibit strong negative ellipticity at 190 nm along with no apparent inflection of the negative band around 218 nm in the considered interval of time.⁴⁷ The experimental CD curves were subjected to deconvolution analysis using the CONTIN and CDSSTR algorithms.⁴⁸ In Figure 2, the graphical representation of the percentage of unordered peptide conformation as estimated at $t = 0$ or $t = 120$ h is reported. The values of the determined random coil secondary structure are reported in Table S1. It is apparent that at $t = 120$ h a higher percentage of random coil conformation is maintained in the presence of the derivative 5 with respect to $A\beta_{42}$ control. The CD spectra of the calix-peptide conjugate 5 alone were recorded in the same experimental conditions. These spectra are characterized by a generalized low CD amplitude that does not change with time (Figure S11). All the above indicates that

5 significantly inhibits the $A\beta_{42}$'s β -sheet conformational transition typically associated with the fibrillogenesis process.⁴⁶ In other words, the CD results suggest that 5 well preserves the $A\beta$ randomly coiled monomer from its recruitment into potentially toxic aggregates. We wanted also to evaluate the ability of the calix[4]arene macrocycle to interfere with the random coil/ β -sheet conformational transition of $A\beta_{42}$. We then acquired a new set of CD measurements, under the same experimental conditions as above, on a sample of $A\beta_{42}$ and the *p*-amino-calix[4]arene derivative 1 in both 1:1 and 1:5 molar ratios. CD data showed that compound 1 is able to interact with $A\beta_{42}$ (Figure S12), although to a lesser extent than 5. This also became evident from the deconvolution analysis (Figure 2) where the percentage of unordered peptide chain is higher than the one of the $A\beta_{42}$ control at $t = 120$ h. The inhibitory effect of the unconjugated GPGKLVFF on $A\beta$'s self-assembly process was also evaluated for comparison. As expected, the CD data demonstrate the ability of the free peptide to interfere with the $A\beta$ aggregation (Figure S13). However, the comparison with the effects generated by the synthesized conjugate 5 allows us to point out some differences. Unlike the case of compound 5, at the 1:1 ratio with $A\beta$, the unconjugated GPGKLVFF peptide is able to accelerate the fibrillogenesis process. This turns evident in the CD experiments (Figure S13). A typical CD profile of the β -sheet conformation was observed after 48 h coincubation ($A\beta$ alone reaches the same conformation after 72 h). The acceleration of the aggregation rate caused massive precipitation, and we were not able to acquire CD spectra at 72 h (Figure S13). The CD data obtained at a 1:5 ratio indicated that the free GPGKLVFF can slow down the aggregation process of $A\beta$ but, in any case, to a lesser extent than the one observed in the presence of the calix-peptide conjugate at both 1:1 and 1:5 ratios. In

conclusion, the CD study suggests that compounds **1** and free GPGKLVFF can affect the $A\beta_{42}$ propensity to adopt β -sheet conformation. Importantly, the CD experiments clearly indicated the superiority of the hybrid system **5** in inhibiting $A\beta_{42}$ aggregation compared to the separate calix or peptide moieties.

Thioflavin T Fluorescence Assay (ThT). The kinetic of $A\beta_{42}$ aggregation was also monitored by ThT fluorescence. ThT is a fluorophore that enhances its fluorescence intensity upon binding to amyloid fibrils.⁴⁹ Fluorescence intensity was monitored at 482 nm for 67 h and at 37 °C. The results are presented in Figure 3. In the absence of inhibitors, $A\beta_{42}$

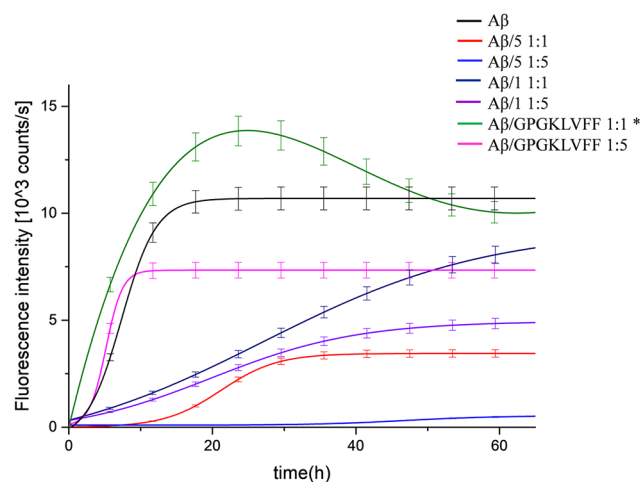


Figure 3. Aggregation kinetics detected by in situ ThT fluorescence assays of $A\beta_{42}$ (20 μ M, black) and in the presence of equimolar or 5-fold molar excess of compound **1**, **5** or GPGKLVFF ($A\beta_{42}/1$ 1:1, dark blue), ($A\beta_{42}/11:5$, purple), ($A\beta_{42}/5$ 1:1, red), ($A\beta_{42}/5$, 1:5 light blue), ($A\beta_{42}/GPGKLVFF$ 1:1, green), ($A\beta_{42}/GPGKLVFF$ 1:5, pink). *The extraction of the kinetic parameters by using the empirical equation in the Experimental Section was not possible.

displayed a rapid increase of the ThT fluorescence, as expected from the inherent propensity to amyloid formation of this peptide. It is also evident that the curve profile observed displays just a hint of initial nucleation phase (Figure 3, black). The prompt formation of aggregated seeds (at $t = 0$) might be the responsible of such behavior. It is assumed that the lower

fluorescence intensity we observed in the presence of the inhibitors at either equimolar ratio or 5-fold molar excess is related to a lesser amount of $A\beta_{42}$ fibrillary aggregated form. The antifibrillogenic activity of the conjugate peptide **5** is evident at equimolar ratio (Figure 3, red). Interestingly the observed profile displays a clear nucleation phase (lag phase), that suggests an effective action of compound **5** in the early events of $A\beta_{42}$ fibrillogenesis.

Such an effect becomes even more apparent at 5-fold molar excess. As one can see, a very long lag phase, along with a negligible increasing of ThT fluorescence intensity, testifies an almost complete inhibition of fibril formation (Figure 3, light blue). The ThT curves related to the kinetic of the calixarene precursor **1** or free GPGKLVFF with $A\beta_{42}$ also reveal the capability of these compounds to interfere with the $A\beta_{42}$ fibrillogenic process, although to a lesser extent than compound **5**. What we observed was a reduction of the fluorescence intensity of the curves, but, again, a clear lag phase was not observed. The only exception was the ThT curve observed at 1:1 ratio for the free GPGKLVFF. It strongly activated $A\beta$ fibril generation (Figure 3, green). This proaggregating behavior is in keeping with the CD measurements, and substantial flocculation appeared after 48 h. The sample reaches ThT fluorescence max intensity faster than $A\beta_{42}$ alone. It might be conceivable that the compound may somehow self-aggregate and give false positive, but control ThT experiments ruled out significant interference occurring between ThT and compounds **1**, **5** or GPGKLVFF (Figure S14). An alternative interpretation implies the ability of free GPGKLVFF compound to become an integral part of ThT positive heterofibrils with $A\beta^{50}$ (Figure 3, pink). The whole of the ThT results further confirm that both **1** and **5** exhibit a dose responsive antifibrillogenic activity. A quantitative analysis of the experimental curves was obtained by proper fitting using a suitable equation, and the relevant kinetic parameters are reported in the Supporting Information (Table S2).

Dynamic Light Scattering (DLS). We resorted to DLS measurements to determine the average size of the aggregates in solution and to monitor their growth over time, either in the absence or in the presence of **5**. Data were collected at $t = 0$ and 120 h and are shown in Figure 4 as the analysis of the number of scattering objects.⁵¹ The analysis indicates that

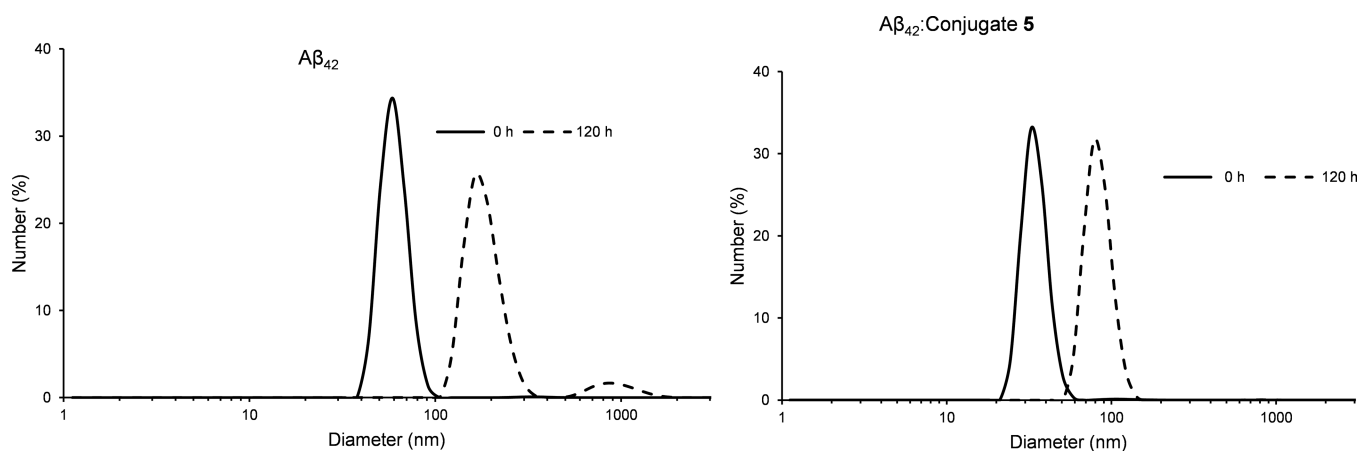


Figure 4. DLS size distributions by number (%) for $A\beta_{42}$ (5 μ M) and $A\beta_{42}$ in the presence of conjugate **5** ($A\beta_{42}/5$ 1:1) at $t = 0$ and after 120 h incubation at 37 °C in 10 mM phosphate buffer.

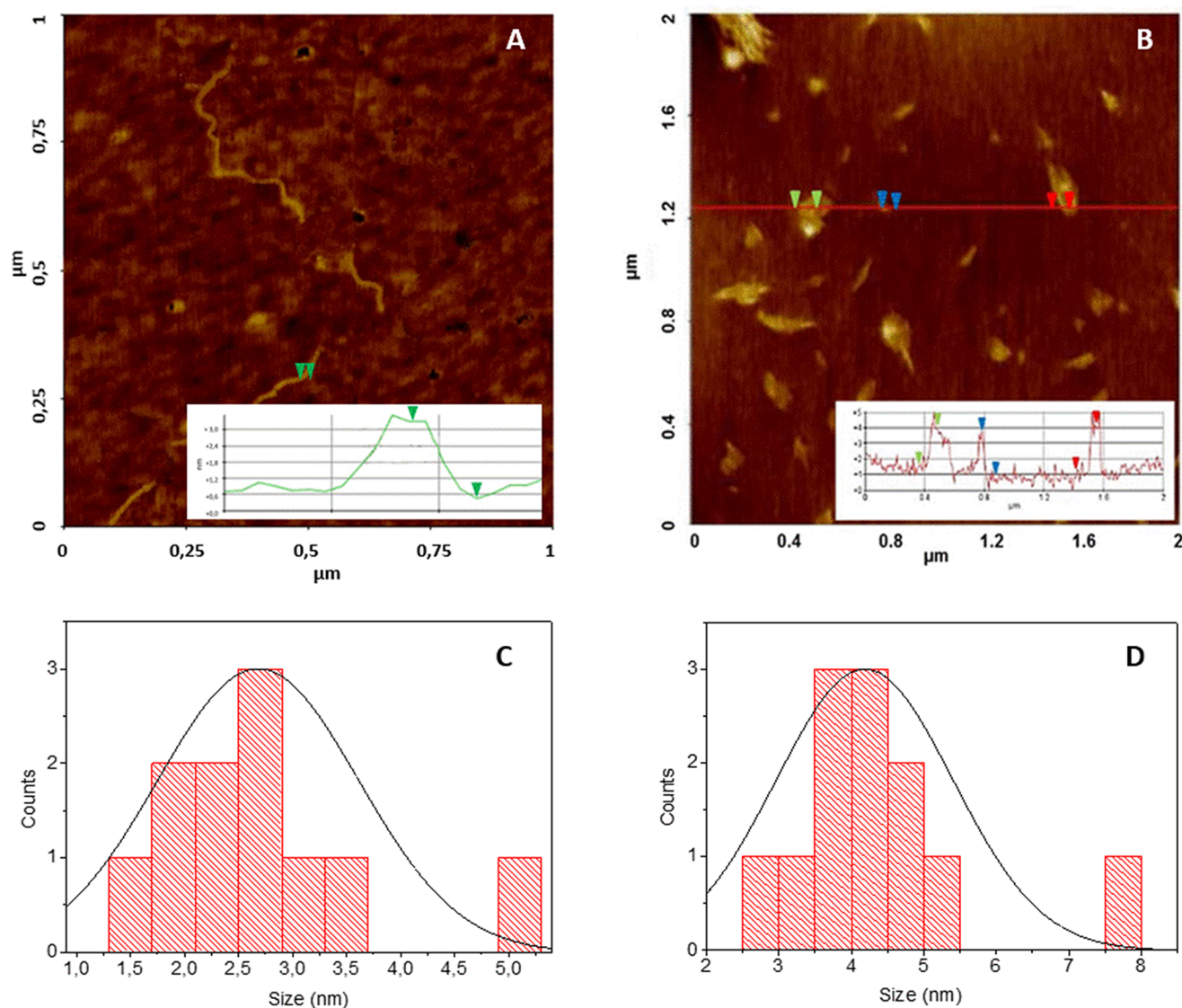


Figure 5. Representative images of AFM analysis for (A) $A\beta_{42}$ alone (5 μM) and (B) copresence of 5 (5 μM) after 120 h. Statistical data for (C) $A\beta_{42}$ (5 μM) and (D) copresence of 5 (5 μM) after 120 h.

small aggregates with an average size of 60 nm are the main scattering objects in the freshly prepared $A\beta_{42}$ sample ($t = 0$). The end stage of $A\beta$ aggregation was analyzed after 120 h, and the formation of larger aggregates was observed. In particular, the DLS profile indicated the presence of particles with increased diameter values (>100 nm) as the most abundant scattering entities, along with a very low percentage of bigger aggregates with size in the micrometric range. The data collected in the presence of 5 clearly indicated the reduction of the dimension of $A\beta_{42}$ aggregates both at the initial stage and end point of monitoring. In fact, at $t = 0$, the majority of the scattering particles in solution displayed a diameter size of around 45 nm (Figure 4), whereas only aggregates as large as 84 nm were detected after 120 h. It should be said that compound 5 alone (5 μM) formed small aggregates with a mean hydrodynamic diameter around 8 nm at $t = 0$. Larger aggregates (diameter > 300 nm) were seen at $t = 120$ h (Figure S15). At 20 μM , compound 5 forms nanoaggregates with a mean hydrodynamic diameter of 22 nm and ζ potential 50 ± 2 mV (Figure S16).

AFM Analysis. Atomic force microscopy (AFM) studies revealed the morphologies of $A\beta_{42}$ aggregates. Figure 5a shows that, after 120 h of incubation, $A\beta_{42}$ (5 μM) alone formed a fibrillary network with an average fibril height of 2.65 ± 0.44 nm. The copresence of 5, at the same concentration (5 μM), during the $A\beta_{42}$ incubation time of 120 h, clearly inhibited the development of amyloid fibrils, and only small amorphous aggregates are detected with sizes of 4.30 ± 1.33 nm (Figure 5b). Statistical data for $A\beta_{42}$ alone and for copresence of 5 are reported in Figure 5c and d, respectively. The AFM images further confirmed the ability of 5 to inhibit $A\beta_{42}$ fibril formation in keeping with the spectroscopic results.

MS Study of $A\beta_{42}$ /5 and $A\beta_{42}$ /GPGKLVFF Interactions. ESI-MS measurements were carried out to verify the formation of molecular adducts when GPGKLVFF and the relative conjugate 5 were added to the $A\beta_{42}$ sample solution. The $A\beta_{42}$ sample and the 1:5 mixtures of $A\beta_{42}$ /5 and $A\beta_{42}$ /GPGKLVFF, were monomerized using the protocol reported in the Experimental Section and lyophilized overnight. The lyophilized sample was dissolved in hexafluoroisopropanol (HFIP) and diluted in H_2O , to obtain a $A\beta_{42}$ final

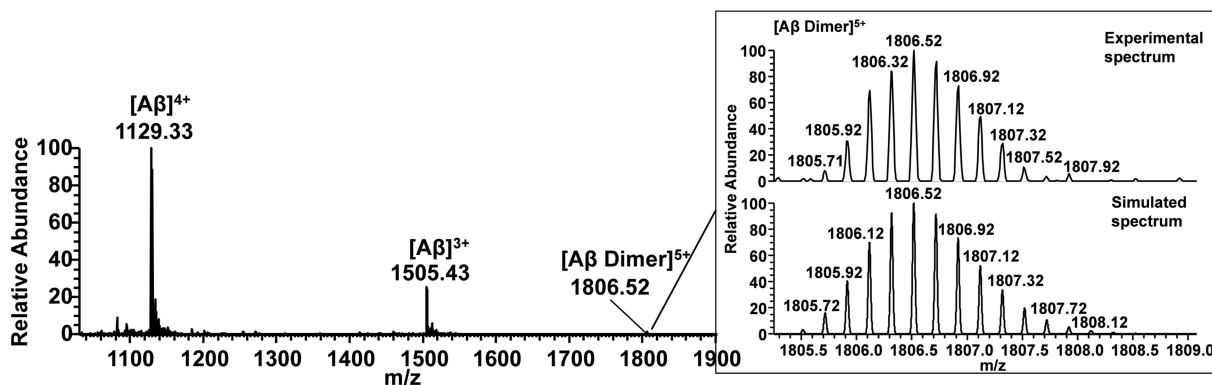


Figure 6. ESI-MS spectrum of $A\beta_{42}$. The inset in the Figure shows the comparison between the experimental and theoretical isotopic distribution of peak corresponding to the $A\beta_{42}$ dimer in the +5 charge state.

concentration of 5.5×10^{-6} M (1% HFIP). The ESI-MS spectrum of $A\beta_{42}$ reported in Figure 6 shows m/z signals at 1129.33 and 1505.43 corresponding to $[A\beta_{42}]^{4+}$ and $[A\beta_{42}]^{3+}$, respectively. A closer inspection of the ESI-MS spectrum revealed a signal at $m/z = 1806.52$ corresponding to the mass of the dimeric peptide in the +5 charge state (Figure 6, inset). This signal disappeared in the mass spectra acquired in the $A\beta_{42}/5$ sample (Figure S17), whereas m/z signals 1507.79 and 2010.06 corresponding to the +4 and +3 charge state of $A\beta_{42}/5$ adduct were observed. Similar effects were seen in the mass spectrum of the $A\beta_{42}/\text{GPGKLVFF}$ sample (Figure S18). Here, m/z signals 1345.20 and 1793.27 can be assigned to the $[A\beta_{42}/\text{GPGKLVFF}]^{4+}$ and $[A\beta_{42}/\text{GPGKLVFF}]^{3+}$ adducts, respectively, with concomitant loss of the dimeric form of $A\beta_{42}$.

Despite the mass spectrometric results were deduced from the gas-phase system, they nicely support what was observed in solution in terms of direct interactions between $A\beta_{42}$ and GPGKLVFF or 5. Nevertheless, this study reveals that the dimeric form of $A\beta_{42}$ is no longer detectable in the MS spectrum when either GPGKLVFF or 5 is present in the sample solution. Such evidence suggests, once more, that these interactions occur in the solution phase and may play a role in the early events of the $A\beta_{42}$ aggregation process. As reported in our previous works,^{16,27} the identification of proteolysis resistant peptide fragments by mass spectrometry may reveal the binding region of $A\beta_{42}$ to specific molecules. Indeed, cleavage of the peptide bonds by a protease is rapid in easily accessible unstructured regions of a polypeptide, whereas the steric hindrance of other molecules at the cleavage sites should affect the rate of hydrolysis. We analyzed the $A\beta_{42}$ peptide fragments generated after 2 h of trypsin digestion. This enzyme selectively catalyzes the hydrolysis of peptide bonds at the C-terminal side of lysyl and arginyl residues. As a matter of fact, the peptide fragments $A\beta(1-5)$, $A\beta(6-16)$, and $A\beta(17-28)$ were detected in the ESI-MS spectrum (see Figure S19), indicating the cleavages expected occur at positions 5, 16, and 28 of $A\beta_{42}$. The peptide fragment $A\beta(1-16)$ was also observed. It could be related to the conformational features of $A\beta_{42}$ that affect the accessibility to the Arg-5-His-6 cleavage site (Scheme S1). The absence of signals corresponding to $A\beta_{42}$ suggested that protein digestion by trypsin was totally accomplished after 2 h (Figure 7a). Interestingly, the peptide fragments $A\beta(17-42)$, $A\beta(6-42)$, and full length $A\beta_{42}$, imputable to incomplete $A\beta_{42}$ processing, were observed in the mass spectra (Figures 7b and 8b, Scheme S2) recorded after 2 h of trypsin digestion in the copresence of 5. Similar

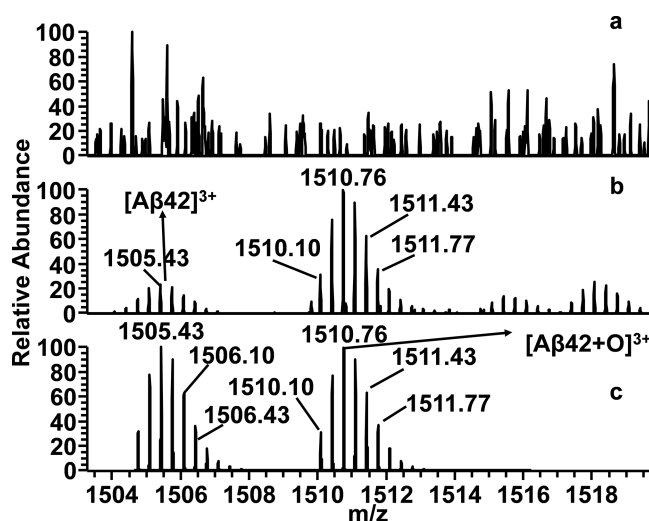


Figure 7. ESI mass spectra of (a) $A\beta_{42}$ sample digested with trypsin and (b) $A\beta_{42}/5$ sample digested with trypsin. (c) Simulated spectrum of $A\beta_{42}$ and oxidized $A\beta_{42}$ form ($A\beta_{42}+O$) for comparative analysis.

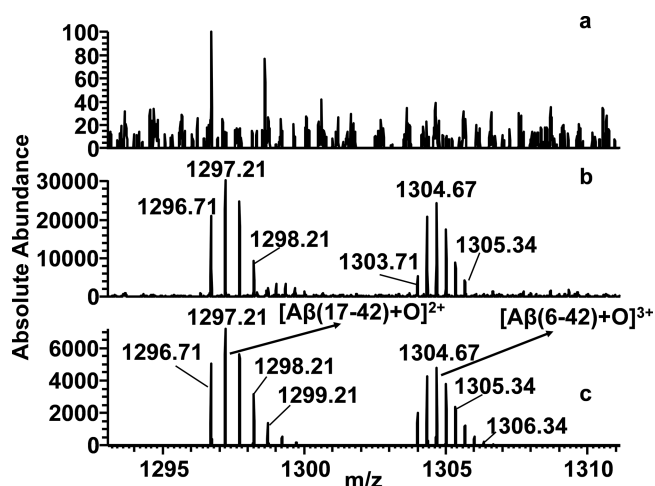


Figure 8. ESI mass spectra recorded at 1293–1311 m/z range of (a) $A\beta_{42}$ sample digested with trypsin and (b) $A\beta_{42}/5$ sample digested with trypsin. (c) Simulated spectrum of $A\beta(17-42)$ and $A\beta(6-42)$ both in the oxidized form for comparative analysis.

results were observed in mass spectra of $A\beta_{42}/\text{GPGKLVFF}$ mixture (data not shown). It is important to note that both GPGKLVFF and 5 were also subjected to trypsin degradation

indicating that these peptides do not inhibit enzyme's activity. Therefore, it can be envisioned that the interaction of GPGKLVFF or 5 with $A\beta_{42}$ affects the processing of the amyloid protein by trypsin. Oxidized forms of $A\beta$ and related fragments were seen in the MS spectra. Oxidation of peptides and proteins during electrospray ionization may occur because the generation of ions in ESI source is related to an electrochemical process.⁵²

Cytotoxicity Studies. Based on the previous promising results, we tested the peptide conjugate 5 for its biological activity in order to (i) exclude any potential toxicity to neuronal cells and more interestingly (ii) assess its ability to prevent oligomers toxicity. For this purpose, we used the neuroblastoma cell line, SH-SY5Y, fully differentiated according to a well-established protocol (see the [Experimental Section](#)). After prolonged treatments with all-*trans*-retinoic acid (RA) and the consequent acquisition of a neuronal-like phenotype, we exposed cells to increasing concentrations of compound 5 (0.1, 5, 20, 50 μM) for 24 h ([Figure 9](#)). The

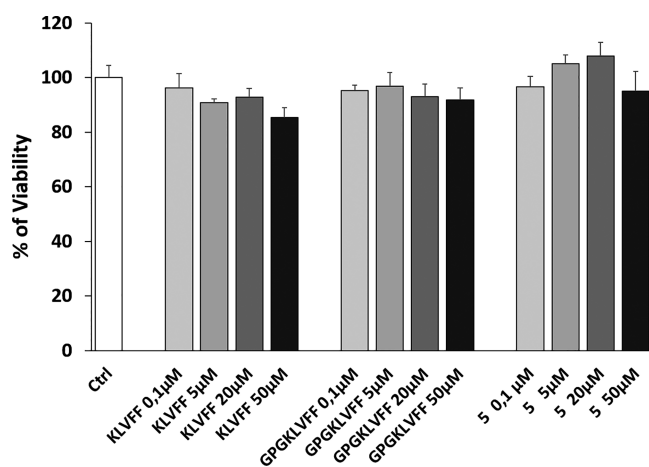


Figure 9. MTT assay was performed on differentiated SH-SY5Y cells after 24 h treatments. Cells were exposed to increasing concentrations of 5 (0.1, 5, 20, 50 μM). Cells were also treated with the same concentrations of appropriate controls (KLVFF or GPGKLVFF). Bars represent means of three independent experiments with $n = 5$.

peptides KLVFF and GPGKLVFF were also added as controls. As expected, the peptide KLVFF as well as the longer peptide containing the tripeptide GPG sequence (GPGKLVFF) revealed similar activity to that of control. Interestingly, no toxicity was observed for compound 5 at any of the concentrations used, with a positive, even if not statistically significant, trend between dose (0.1–20 μM) and cellular response, after 24 h exposure. Hence, we tested the ability of compound 5 to protect neurons from the $A\beta_{42}$ oligomer cytotoxic insult. $A\beta$ oligomers ($\alpha A\beta$ s) were obtained from freshly prepared solution of $A\beta_{42}$, incubated for 48 h at 4 $^{\circ}\text{C}$ in the presence or in the absence of the calixarene–peptide conjugate 5.

$A\beta$ oligomers obtained following the incubation were added at the final concentration of 2 μM , alone or in combination with all of the compounds at the molar ratios of 1:1 and 1:5. Cells were then exposed for 48 h to each coincubated mixture and cell viability was quantified by MTT assay. As shown in [Figure 10](#), $A\beta$ oligomers induce a slight but statistically significant reduction of cell viability that is clearly prevented in the presence of compound 5. We have already reported on the

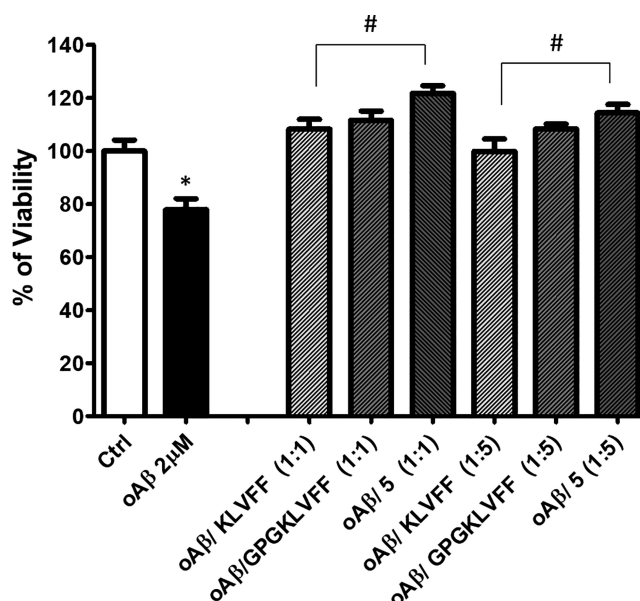


Figure 10. MTT assay was performed on differentiated SH-SY5Y cells after 48 h treatments. Cells were exposed to 2 μM $A\beta$ oligomers incubated with or without compound 5 at the molar ratios of 1:1 and 1:5. Coincubations with KLVFF alone and GPGKLVFF were also performed as experimental controls. Bars represent means \pm SEM of three independent experiments with $n = 3$. * $P < 0.05$ vs control by one-way ANOVA + Tukey test. # $P < 0.05$ vs $\alpha A\beta$ by one-way ANOVA + Tukey test.

antiloligomerization activity of a trehalose conjugated LPFFD peptide.⁵³ The newly synthesized compound shows a similar interesting effect of the $A\beta$ derived pentapeptide with a better trend, making this functionalization even more promising also in the light of calix[4]arenes ability to be potentially loaded with selected drugs. The biological effect observed on SH-SY5Y differentiated cells has been also confirmed by SDS-polyacrylamide gel experiments. The same solutions used to treat the cells were in fact loaded onto 4–12% gel polyacrylamide to assess the amount and size of $A\beta_{42}$ aggregates formed in the presence of the compound 5 or its related controls. Two different concentrations of $A\beta_{42}$ have been used and each peptide added with a molar ratio of 1:5. Results show that, as expected, $A\beta$ alone during 48 h incubations at 4 $^{\circ}\text{C}$ was able to give rise to the typical migration pattern in which low molecular weight size (LMW: monomers, dimers, and tetramers) and high molecular weight (HMW: >50 kDa oligomers) size are observed ([Figure S20](#)). Coincubation with compound 5 strongly decreases the HMW band signal, which confirmed that our compound interferes with $A\beta$ aggregation.

CONCLUSION

In the present work, we have described the design, synthesis, and biophysical properties of a new calixarene–peptide construct that combines the $A\beta$ recognition ability of the GPGKLVFF sequence with the host and recognition properties of the calixarene macrocycle. This novel compound is able to prevent cross- β -sheet elongation of $A\beta_{42}$ through a synergistic action of both calixarene and peptide moieties that can be considered as β -sheet breaker elements. This is an interesting example of a small construct being able to preserve the nontoxic monomeric species of $A\beta_{42}$ from being recruited

into oligomeric/fibrillar aggregated forms, as demonstrated by circular dichroism and ThT fluorescence. The lack of toxicity, combined with the significant protective action on neuronal cells, further points toward a considerable therapeutic potential of this novel construct. Moreover, given the already established pharmaceutical functions of calixarenes in drug delivery, our findings suggest that the conjugate has great potential as a vehicle for the targeted delivery of additional therapeutic agents in AD. In fact, due to the presence of calix[4]arene and peptide moieties, multiple potential actions can be expected, and the possibility that the calixarene cavity offers to host and transport a variety of guests, such as drugs or imaging agents, opens up interesting perspectives for further investigations in diagnosis and therapy for amyloid related diseases. The calix[*n*]arene family offers a variety of macrocyclic scaffolds differing in size and structural conformation that, together with the versatility and ease of functionalization, may provide an additional tool for the development of other peptide–calixarene conjugates for A β aggregation inhibitors.

EXPERIMENTAL SECTION

Materials and Instrumentation. All the reagents were of analytical grade. Calix[4]arene derivative **1**⁴⁴ and GPGKLVFF peptide were prepared according to standard chemical procedures reported below. A β ₄₂ was obtained from Bachem (Switzerland). MALDI-TOF spectra were recorded on the SCIEX TOF/TOF 5800 instrument. The MALDI-MS spectra were carried out using α -CHCA as a matrix with a thin layer deposition method. Lyophilized samples (0.1 mg) were dissolved in 100 μ L of 1:1:0.01 acetonitrile/water/TFA. Sinapinic acid (SIN) and α -CHCA were prepared by dissolving 4–8 mg/vial of matrices in 1 mL of 50% acetonitrile in 0.3% TFA and 1 mL of 30% acetonitrile in 0.3% TFA, respectively. Standard kits were used to calibrate the mass scale of the MALDI mass spectrometer. The Peptide Mass standard kit includes des-Arg1-bradikynin, angiotensin I, Glu1-fibrinopeptide B, ACTH (Clip 1–17), ACTH (Clip 18–39), and ACTH (Clip 7–38), and it was used to cover a mass range of 800–4000 Da.

¹H NMR (400.13 MHz), ¹³C NMR (100.61 MHz), and 2D NMR spectra were acquired on a Bruker Avance 400 spectrometer. Chemical shifts (δ) are expressed in parts per million (ppm), referenced to the residual methanol peak; coupling constant (*J*) values are given in Hz.

Synthesis of GPGK(Dde)LVFF. The peptide was synthesized using the microwave assisted solid phase peptide synthesis strategy on a Liberty Peptide Synthesizer (CEM). The peptide chain assembly was carried out on a NovaSyn TGR resin (substitution 0.22 mmol/g) using the Fmoc chemistry method. All Fmoc-amino acids were introduced according to the TBTU/HOBT/DIEA or COMU activation methods. All syntheses were carried out under a 4-fold excess of amino acid. Removal of Fmoc protection during synthesis was achieved by means of 20% piperidine solution in DMF. The following instrumental conditions were used for each coupling cycle: microwave power 25 W, reaction temperature 75 °C, coupling time 300 s. The instrumental conditions used for the deprotection cycles were: microwave power 25 W, reaction temperature 75 °C, deprotection time 180 s. The peptides were cleaved off from the resin using a mixture of TFA/H₂O/TIS (95:2.5:2.5 v/v/v). Crude peptides were recovered by precipitation with freshly distilled diethyl ether. The purification of crude GPGK(Dde)LVFF was carried out by preparative reversed-phase HPLC using a SHIMADZU LC-20A chromatography system equipped with a SPD-M20A photodiode diode array detector with detection at 222 and 254 nm. A Kinetex C18 250 \times 21.10 mm (100 Å pore size, AXIA Packed) column was used. The peptides were eluted at a flow rate of 10 mL/min according to the following protocol: from 0 to 5 min isocratic conditions in 95% solvent A (H₂O containing 0.1% TFA) followed by a 20 min linear gradient from 5 to 70% B (CH₃CN containing 0.1% TFA) and then 5

min isocratic conditions in 70% B. Fractions containing the desired product were collected and lyophilized. Sample identity was confirmed by ESI-ORBITRAP MASS. Calculated mass: 1026.59; observed: [M + H]⁺ = 1027.59; [M + 2H]²⁺ = 514.30.

Synthesis of 5,11,17,23-Tetra-Boc-amino-25,26,27-tripropoxy-28-(2-ethoxycarbonylmethoxy)-calix[4]arene (2). To compound **1** (200 mg, 0.29 mmol) dissolved in passed through basic alumina CH₂Cl₂ (8 mL), di-*tert*-butyl dicarbonate (0.33 mL, 1.44 mmol) was added. The mixture was stirred at rt overnight, then a 5% aq NaHCO₃ solution (50 mL) and CH₂Cl₂ (50 mL) were added. The organic phase was washed with 5% aq NaHCO₃ solution (50 mL) and water (50 mL \times 2). After removal of the solvent under vacuum, the solid residue was washed with hexane and recovered by filtration to give pure compound **2** (283 mg, 90%). ¹H NMR (CDCl₃, 297 K) δ : 0.92 (t, 3H, *J* = 7.4 Hz, propyl CH₃), 0.98 (t, 6H, *J* = 7.4 Hz, 2 \times propyl CH₃), 1.26 (t, 3H, *J* = 7.1 Hz, OCH₂CH₃), 1.46, 1.49, (s, 9H each, Boc CH₃), 1.56 (s, 18H, 2 \times Boc CH₃), 1.85 (m, 6H, *J* = 7.4 Hz, 3 \times propyl CH₂CH₃), 3.08 and 4.37 (AX system, 4H, *J* = 13.4 Hz, 2 \times ArCH₂Ar), 3.14 and 4.57 (AX system, 4H, *J* = 13.4 Hz, 2 \times ArCH₂Ar), 3.71 (t, 4H, *J* = 7.4 Hz, 2 \times propyl OCH₂), 3.80 (t, 2H, *J* = 7.4 Hz, propyl OCH₂), 4.17 (q, 2H, *J* = 7.1 Hz, OCH₂CH₃), 4.64 (s, 2H, OCH₂CO), 6.03 (s, 2H, 2 \times ArH), 6.26 (d, 2H, *J* = 3.4 Hz, 2 \times ArH), 6.43 (d, 2H, *J* = 3.4 Hz, 2 \times ArH), 6.81 (s, 2H, 2 \times ArH).

Synthesis of 5,11,17,23-Tetra-Boc-amino-25,26,27-tripropoxy-28-(carbomethoxy)-calix[4]arene (3). Compound **2** (100 mg, 0.075 mmol) was suspended in THF (10 mL) in the presence of water (2 mL) and KOH (50 mg, 0.89 mmol). The resulting mixture was refluxed and stirred for 3 h. The pH was adjusted to 4 with aq 1 N HCl. The product was extracted with CH₂Cl₂, and the organic layer was dried over Na₂SO₄ and evaporated to give pure compound **3** (95.37 mg, 98%). ¹H NMR (MeOD, 297 K) δ : 0.91 (t, 3H, *J* = 7.4 Hz, propyl CH₃), 1.02 (t, 6H, *J* = 7.4 Hz, 2 \times propyl CH₃), 1.42, 1.51, (s, 18H each, Boc CH₃), 1.88 (m, 6H, *J* = 7.4 Hz, 3 \times propyl CH₂CH₃), 3.12 and 4.40 (AX system, 4H, *J* = 12.7 Hz, 2 \times ArCH₂Ar), 3.18 and 4.45 (AX system, 4H, *J* = 12.7 Hz, 2 \times ArCH₂Ar), 3.73 (t, 4H, *J* = 7.4 Hz, 2 \times propyl OCH₂), 3.95 (t, 2H, *J* = 7.4 Hz, propyl OCH₂), 4.68 (s, 2H, OCH₂CO), 6.58 (s, 4H, 4 \times ArH), 7.08 (s, 4H, 4 \times ArH).

Synthesis of p-Boc-amino-calix[4]arene-GPGKLVFF-Dde Conjugate (4) and Deprotection to p-Amino-calix[4]arene-GPGKLVFF Conjugate (5). To 20 mg of calixarene derivative **3** (0.018 mmol) dissolved in 2 mL of dry DMF, pyBop (16.8 mg, 0.031 mmol) and DIPEA (10.5 μ L, 0.061 mmol) were added. The mixture was stirred for 2 h at room temperature, and then GPGK(Dde)LVFF (20.9 mg, 0.020 mmol) dissolved in DIPEA (5.6 μ L, 0.032 mmol) was added. After stirring at room temperature for 18 h, the solvent was removed under vacuum, the solid was washed by centrifugation, three times with diethyl ether and two times with 0.01 N HCl. The residue was dried *in vacuo*. Pure compound **4** (15 mg, 0.0072 mmol, 40% yield) was obtained by preparative TLC (MeOH/CH₂Cl₂, 5:95 v/v). The Dde protecting group was removed from compound **4** by treatment with 2% hydrazine (1 mL), under stirring, at rt, for 30 min. After removal of hydrazine under vacuum, 20% TFA in CH₂Cl₂ (1 mL) was added to the solid, for removing the Boc groups. The mixture was stirred at room temperature for 2 h. The solvent was removed under vacuum, and the solid was washed three times with diethyl ether by centrifugation, to give pure compound **5** after freeze drying (11.4 mg, 95% yield). Sample identity was confirmed by MALDI-TOF mass spectrometry. Calculated mass for C₈₃H₁₁₂N₁₄O₁₃: 1512.8533; observed: 1536.0288 (M + Na)⁺; 1551.9912 (M + K)⁺. ¹H NMR (CDCl₃/MeOD 1:3 v/v, 297 K) δ 0.70 (d, 3H, *J* = 6.7 Hz, CH₃ Val), 0.80 (d, 3H, *J* = 6.7 Hz, CH₃ Val), 0.87 (d, 3H, *J* = 6.5 Hz, CH₃ Leu), 0.88 (d, 3H, *J* = 6.5 Hz, CH₃ Leu), 0.93 (t, 6H, *J* = 7.5 Hz, 2 \times CH₃ propyl), 0.96 (t, 3H, *J* = 7.5 Hz, CH₃ propyl), 1.27 (m, 2H, *J* = 7.5 Hz, CH₂ Lys), 1.44–1.60 (m, 3H, CH₂ Lys and CH Leu), 1.60–1.90 (overlapped, 10H, CH₂ Lys, CH₂ Leu, 3 \times CH₂ propyl), 1.90–2.00 (m, 1H, *J* = 6.7 Hz, CH Val), 2.00–2.10 (m, 2H, CH₂ Pro), 2.13 and 2.24 (m, 1H each, CH₂ Pro), 2.80 (m, 2H, CH₂ Lys), 2.80–3.20 (8 dd, 2H, CH₂ Pro), 3.20–3.43 (overlapped, 8H, 2 \times ArCH₂Ar calixarene, and 2 \times CH₂ Phe), 3.71–3.93 (m, 6H, 3 \times OCH₂ propyl),

3.96 (d, J = 6.8 Hz, 1H, Val CH), 4.10 (d, 1H, 1 × CH₂ Gly) 4.20–4.36 (m overlapped, 2H, CH Leu and CH Lys), 4.36–4.61 (overlapped, 13H, 1 × CH₂ Gly, CH₂ Gly, ArOCH₂CO, 2 × ArCH₂Ar calixarene, CH Prol, CH Leu, 2 × CH Phe), 6.34 (br s, 4H, 2 × ArNH₂ calixarene), 6.38 (s, 2H, 2 × ArH calixarene), 6.46 (br s, 2H, ArNH₂ calixarene), 6.66 (br d, 4H, 4 × ArH calixarene), 6.70 (br s, 2H, ArNH₂ calixarene), 6.79 (s, 2H, 2 × ArH calixarene), 7.09–7.37 (overlapped, 10H, 5 × ArH Phe). ¹³C NMR (CDCl₃/MeOD 1:3 v/v, 297 K): 10.5, 10.8 (q), 18.9, 19.4, 21.8, 21.9 (q), 23.4, 23.6, 24.0, 25.0 (d), 25.7, 27.4, 30.3, 38.2, 38.5, 40.3, 40.8, 42.4, 44.2 (t), 54.2, 54.6, 55.9, 56.5, 61.1, 62.2 (d), 74.7, 77.9 (t), 122.1, 123.2, 127.6, 127.7, 129.3, 129.4, 130.0, 130.2 (d), 136.6, 136.7, 137.1, 138.0, 138.3 (s), 169.3, 171.9, 172.1, 172.9, 173.4, 174.3, 175.1, 175.6 (s, CO).

Sample Preparation. Aβ₄₂ was dissolved in TFA (1 mg/mL) and sonicated for 10 min. Then the TFA was removed under a gentle stream of N₂, 1 mL of HFIP was added, and the mixture was dried under N₂ stream to remove the remaining trace of TFA (×2). Aβ₄₂ was again dissolved in 1 mL of HFIP and was frozen at –70 °C and then lyophilized overnight. The same procedure was carried out in the presence of conjugate 5.

Circular Dichroism Spectroscopy. CD spectra were acquired using a J-810 spectrometer (Jasco, Japan) under a constant flow of N₂ at room temperature. The CD spectra were recorded for Aβ₄₂ (5 μM) monomer in the absence and presence of 1 and 5 (5 and 25 μM). The lyophilized samples were dissolved in 50 μL of 10 mM NaOH and then diluted with 10 mM phosphate buffer pH 7.4 containing 100 mM NaCl to 2 mL to obtain a concentration 5 μM for Aβ₄₂ alone and the mixture of Aβ₄₂ and conjugate 5 (1:1 and 1:5 molar ratio). A 1 cm path length quartz cuvette was used to acquire the far-UV CD spectra (190–260 nm) at a scan speed of 50 nm/min. There were 10 scans collected. The CD signal of the solution without Aβ₄₂ was subtracted from the sample CD spectra. The measurements were performed in triplicate.

Thioflavin T Fluorescence Assay. ThT fluorescence kinetics were measured on a Flash Thermo Variokan spectrofluorometer with excitation and emission at 450 and 480 nm, respectively. Aβ₄₂ alone and in the presence of the conjugates 1 or 5 in 1:1 or 1:5 molar ratio was dissolved in 10 mM aq NaOH (30 μL). The samples were diluted (to 150 μL) with 60 μM ThT solution in 10 mM phosphate buffer at pH 7.4 to obtain a final Aβ₄₂ concentration of 20 μM. The samples were incubated at 37 °C in a 96-well plate. To minimize evaporation effects the multiwell plate was sealed with a transparent heat-resistant plastic film. Readings were taken every 10 min, after weak shaking for 10 s. The fluorescence intensity was monitored for 67 h. The measurements were performed in triplicate. To minimize errors during sample preparation, we freeze dried the aliquots of monomerized Aβ₄₂ and 5 directly into each well of the plate. The experimental data were fitted by using the equation:

$$F(t) = F_0 + \frac{F_{\max} - F_0}{1 + e^{-t-t_{1/2}/k}}$$

where F_0 is the initial fluorescence emission and F_{\max} is the final increment of fluorescence emission; $1/k$ is the elongation rate constant, and $t_{1/2}$ is the time at which the amplitude of ThT emission is 50% of the F_{\max} value. t_{lag} is defined as the intercept between the time axis and the tangent of the curve with slope k from the midpoint of the fitted sigmoidal curve; this parameter was calculated from the fitted parameters by using the following equation: $t_{\text{lag}} = t_{1/2} - 2k$.

The kinetic parameters are expressed as the mean (±SD) of three independent experiments.

Dynamic Light Scattering (DLS) and Electrophoretic Light Scattering (ELS). DLS and ELS measurements were carried out on a ZetaSizer NanoZS90 Malvern instrument (UK), equipped with a 633 nm laser at a scattering angle of 90° and 25 °C temperature. The size of Aβ₄₂, conjugate 5, and Aβ₄₂ in the presence of 5 was determined on samples prepared at the same experimental conditions as CD analyses. Each measurement was performed three times.

Atomic Force Microscopy. AFM analysis was performed with a PSIAXE-150 system, acquiring images of 1 × 1 and 2 × 2 μm². The measurements were carried out in tapping mode using a silicon Sn

doped tip (resistivity of 0.01 Ω cm and purchased by Bruker TESPA). New cantilevers were used for each measurement. Tip dimensions: thickness 4 μm, length 125 μm, width 40 μm. The stiffness was 40 N/m, and the tip was operated to an oscillation frequency of 320 kHz. An aliquot with a volume of 10 μL of sample was dispensed on a precleaned silicon flat substrate and dried. In order to perform a representative investigation of whole samples, after deposition the substrates were not rinsed with Milli-Q water (as commonly reported in literature). For each sample, various areas on the sample were investigated and statistically relevant images were chosen.

Mass Spectrometry Analyses. The lyophilized Aβ₄₂ was dissolved in HFIP (hexafluoroisopropanol) to obtain a concentration of 2.2 × 10^{−4} M (Aβ₄₂ stock solution). The GPGKLVFF peptide and compound 5 were dissolved in HFIP to obtain a stock solution of 1.1 × 10^{−3} M for each. The Aβ₄₂ sample and the mixtures of Aβ₄₂/GPGKLVFF and Aβ₄₂/5 at 1:5 ratios, were prepared from stock solutions to a final concentration [Aβ₄₂] = 5.5 × 10^{−6} M, [5] = [GPGKLVFF] = 27.5 × 10^{−6} M in Milli-Q water at physiological pH. For proteolysis experiments, 25 × 10^{−6} g of trypsin enzyme was dissolved in HCl 1 × 10^{−3} M [trypsin] = 2.14 × 10^{−5} M, and then an appropriate volume of the enzyme stock solution was added to the Aβ₄₂, Aβ₄₂/GPGKLVFF, and Aβ₄₂/5 samples to obtain a final enzyme/substrate ratio of 1:20 w/w. Solutions were incubated at 37 °C, and then the digestion reactions were stopped after 2 h by adding 1 μL 0.3% aqueous TFA. The samples were analyzed by using an ESI-MS Orbitrap Q-exactive system (Thermo Scientific). Each sample was introduced into the ESI source on 100 mm internal diameter fused silica via a 500 mL syringe. Full MS scans in the m/z range 400–4000 were acquired in the positive ion mode, spray voltage = 3.5 kV, capillary temperature = 300 °C; m/z range = 400–4000, S-lens RF level = 60 V, sheath gas = 7, resolving power: 70 000 fwhm. The spectra, recorded as raw files, were imported in Qual Browser (Thermo Scientific) software for analysis. Averaged MS spectra were imported into a freely available open-source software, mMass (<http://www.mmass.org>). Theoretical m/z values of Aβ₄₂, GPGKLVFF, 5, the adducts Aβ₄₂/GPGKLVFF and Aβ₄₂/5, and the peptides resulting from in silico digestion of Aβ₄₂ were compared with the m/z values assigned to experimental mass spectra. Peptides that matched successfully, within a tolerance of 0.005 Da, were annotated.

Cell Cultures and MTT Assay. The neuroblastoma (NB) cell line, SH-SY5Y, was maintained in DMEM-F12 (Gibco, ThermoFisher) supplemented with 10% heat inactivated (HI) fetal calf serum (Gibco, ThermoFisher), 100 mg/mL penicillin and streptomycin (Gibco, ThermoFisher), and 2 mM L-glutamine at 37 °C, 5% CO₂. Two weeks before experiments, 5 × 10⁵ cells were plated on 96-well plates in DMEM-F12 with 5% HI fetal calf serum. The percentage of serum was gradually decreased until it was 1% of the total. All-trans-retinoic acid (RA) (Sigma), 5 μM, was used to promote neuronal differentiation, and medium-containing RA was changed every 3 days. Treatments with compound 5, KLVFF, and GPGKLVFF were performed on fully differentiated cells. After 24 h treatment, cultures were incubated with MTT (0.5 mg/mL) for 2 h at 37 °C and then lysed with DMSO, and the formazan production was evaluated in a plate reader through the absorbance at 570 nm.

Antiligomerization Assay. Aβ₄₂ oligomers were prepared as previously described⁵³ from synthetic Aβ₄₂ following a protocol for monomerization. An amount of 1 mg of Aβ₄₂ was first dissolved in 5 mM DMSO. A solution of 10 μM Aβ₄₂ in ice-cold DMEM F-12 without Phenol Red was prepared and allowed to oligomerize for 48 h at 4 °C according to the Lambert protocol⁵⁴ with some modification as previously described.⁵⁵ In order to evaluate the ability of compound 5 and the other appropriate controls (KLVFF, GPGKLVFF), samples of Aβ₄₂ (10 μM) were incubated in the presence or absence of each compound (Aβ/ligand ratios 1:1, 1:5). After 48 h incubation, Aβ/ligand compounds were applied to the differentiated SH-SY5Y cells at the final concentration of 2 μM Aβ.

Western Blot Analysis. A stock aliquot of 5 mM Aβ previously dissolved in DMSO was diluted in DMEM F-12 without Phenol Red, and two different samples at 20 μM and 50 μM concentrations were prepared. From each solution, two sets of samples were obtained by

combining $A\beta_{42}$ with KLVFF peptide, GPGKLVFF, or compound 5 with a molar ratio $A\beta$ /peptide of 1:5. All the samples, including $A\beta$ alone at the two concentrations used, were incubated at 4 °C for 48 h to form $A\beta$ oligomers. After incubation, the amount and size of $A\beta$ aggregates were determined by Western blot analysis. A volume of 25 μ L of each unheated sample was loaded onto a precast Bis-Tris gel (Bolt 4–12%, Life Technologies) with 2-morpholin-4-yl ethanesulfonic acid (MES). Samples were transferred onto a nitrocellulose membrane (0.2 mm, Hybond ECL, Amersham Italia) by using a wet transfer unit Mini Blot Module (Life Technologies). Membranes were blocked in Odyssey blocking buffer (LI-COR Biosciences) and incubated at 4 °C overnight with mouse monoclonal anti-amyloid- β antibody against N-terminal 1–16 peptide (1:1000) (Covance). A secondary goat anti-mouse antibody labeled with IR dye 800 (1:25 000) was used at rt for 45 min. Hybridization signals were detected with the Odyssey CLx infrared imaging system (LI-COR Biosciences, Lincoln, NE).

■ ASSOCIATED CONTENT

SI Supporting Information

The Supporting Information is available free of charge at <https://pubs.acs.org/doi/10.1021/acschemneuro.1c00117>.

Tables containing values of random coil secondary structures and ThT kinetic parameters, MS, NMR, CD, ThT spectra, DLS and ELS measurements; Western blot analysis (PDF)

■ AUTHOR INFORMATION

Corresponding Authors

Giuseppe Pappalardo – CNR-Institute of Crystallography, 95126 Catania, Italy; orcid.org/0000-0001-7328-3492; Email: giuseppe.pappalardo@cnr.it

Grazia Maria Letizia Consoli – CNR-Institute of Biomolecular Chemistry, 95126 Catania, Italy; orcid.org/0000-0003-4189-930X; Email: grazia.consoli@icb.cnr.it

Authors

Rita Tosto – International PhD School of Chemical Sciences, University of Catania, 95125 Catania, Italy; CNR-Institute of Crystallography, 95126 Catania, Italy

Ausilia Baglieri – CNR-Institute of Biomolecular Chemistry, 95126 Catania, Italy

Salvatore Petralia – Department of Drug Sciences and Health, University of Catania, 95125 Catania, Italy; orcid.org/0000-0001-5692-1130

Tiziana Campagna – CNR-Institute of Crystallography, 95126 Catania, Italy

Giuseppe Di Natale – CNR-Institute of Crystallography, 95126 Catania, Italy

Stefania Zimbone – CNR-Institute of Crystallography, 95126 Catania, Italy

Maria Laura Giuffrida – CNR-Institute of Crystallography, 95126 Catania, Italy

Complete contact information is available at:

<https://pubs.acs.org/doi/10.1021/acschemneuro.1c00117>

Author Contributions

G.P. designed the research, supervised data, and wrote the paper; G.M.L.C. designed the research and performed calixarene synthesis, calix-peptide conjugation, and DLS measurements; R.T. performed peptide synthesis and CD and ThT measurements; A.B. performed calixarene synthesis, calix-peptide conjugation, and DLS measurements; S.P. performed AFM measurements; T.C. performed CD measurements;

G.D.N. performed MS analysis; S.Z. and M.L.G. performed biological experiments.

Notes

The authors declare no competing financial interest.

■ ACKNOWLEDGMENTS

Authors thank Regione Sicilia – Dipartimento regionale dell'Istruzione e della Formazione Professionale- Avviso pubblico N.11/2017 FSE Fondo Sociale Europeo Programma Operativo Sicilia 2014–2020 “Rafforzare l'occupabilità nel sistema della R&S e la nascita di spin-off di ricerca in Sicilia”. Project TE(A)CH for financial support.

■ REFERENCES

- (1) Tóth, P., Gavurová, B., and Barták, M. (2018) Alzheimer's disease mortality according to socioeconomic factors: Country Study. *Int. J. Alzheimer's Dis.* 2018, 1–12.
- (2) Armstrong, A. R. (2019) Risk factors for Alzheimer's disease. *Folia Neuropathol.* 57, 87–105.
- (3) Hardy, J., and Selkoe, D. J. (2002) The amyloid hypothesis of Alzheimer's disease: Progress and problems on the road to therapeutics. *Science* 297, 353–356.
- (4) Stefani, M., and Dobson, C. M. (2003) Protein aggregation and aggregate toxicity: New insights into protein folding, misfolding diseases and biological evolution. *J. Mol. Med.* 81, 678–699.
- (5) Cheignon, C., Tomas, M., Bonnefont-Rousselot, D., Faller, P., Hureau, C., and Collin, F. (2018) Oxidative stress and the amyloid Beta peptide in Alzheimer's disease. *Redox Biol.* 14, 450–464.
- (6) Darling, A. L., and Shorter, J. (2020) Atomic structures of amyloid- β oligomers illuminate a neurotoxic mechanism. *Trends Neurosci.* 43, 740–743.
- (7) Ciudad, S., Puig, E., Botzanowski, T., Meigooni, M., Arango, A. S., Do, J., Mayzel, M., Bayoumi, M., Chaignepain, S., Maglia, G., Cianferani, S., Orekhov, V., Tajkhorshid, E., Bardiaux, B., and Carulla, N. (2020) $A\beta(1-42)$ tetramer and octamer structures reveal edge conductivity pores as a mechanism for membrane damage. *Nat. Commun.* 11, 3014–3028.
- (8) Cox, S. J., Lam, B., Prasad, A., Marietta, H. A., Stander, N. V., Joel, J. G., Sahoo, B. R., Guo, F., Stoddard, A. K., Ivanova, M. I., and Ramamoorthy, A. (2020) High-throughput Screening at the Membrane Interface Reveals Inhibitors of Amyloid- β . *Biochemistry* 59, 2249–2258.
- (9) Sahoo, B. R., Cox, S. J., and Ramamoorthy, A. (2020) High-resolution probing of early events in amyloid- β aggregation related to Alzheimer's disease. *Chem. Commun.* 56, 4627–4639.
- (10) Brender, J. R., Ghosh, A., Kotler, S. A., Krishnamoorthy, J., Bera, S., Morris, V., Sil, T. B., Garai, K., Reif, B., Bhunia, A., and Ramamoorthy, A. (2019) Probing transient non-native states in amyloid beta fiber elongation by NMR. *Chem. Commun.* 55, 4483–4486.
- (11) Wang, Q., Yu, X., Li, L., and Zheng, J. (2014) Inhibition of amyloid- β ; aggregation in Alzheimer's disease. *Curr. Pharm. Des.* 20, 1223–1243.
- (12) Giuffrida, M. L., Caraci, F., Pignataro, B., Cataldo, S., De Bona, P., Bruno, V., Molinaro, G., Pappalardo, G., Messina, A., Palmigiano, A., Garozzo, D., Nicoletti, F., Rizzarelli, E., and Copani, A. (2009) β -Amyloid monomers are neuroprotective. *J. Neurosci.* 29, 10582–10587.
- (13) Doig, A. J., and Derreumaux, P. (2015) Peptide inhibitors of beta-amyloid aggregation. *Curr. Opin. Struct. Biol.* 30, 50–56.
- (14) Jokar, S., Khazaei, S., Behnammanesh, H., Shamloo, A., Erfani, M., Beiki, D., and Bavi, O. (2019) Recent advances in the design and applications of amyloid- β peptide aggregation inhibitors for Alzheimer's disease therapy. *Biophys. Rev.* 11, 901–925.
- (15) Sinopoli, A., Giuffrida, A., Tomasello, M. F., Giuffrida, M. L., Leone, M., Attanasio, F., Caraci, F., De Bona, P., Naletova, I., Saviano, M., Copani, A., Pappalardo, G., and Rizzarelli, E. (2016) Ac-LPFFD-

Th: A trehalose-conjugated peptidomimetic as a strong suppressor of amyloid- β Oligomer Formation and Cytotoxicity. *ChemBioChem* 17, 1541–1549.

(16) Di Natale, G., Zimbone, S., Bellia, F., Tomasello, M. F., Giuffrida, M. L., Pappalardo, G., and Rizzarelli, E. (2018) Potential therapeutics of Alzheimer's diseases: New insights into the neuroprotective role of trehalose-conjugated beta sheet breaker peptides. *Pept. Sci.* 110, No. e24083.

(17) Savelieff, M. G., Liu, Y., Senthamarai, R. R. P., Korshavn, K. J., Lee, H. J., Ramamoorthy, A., and Lim, M. H. (2014) A small molecule that displays marked reactivity toward copper- versus zinc-amyloid- β implicated in Alzheimer's disease. *Chem. Commun.* 50, 5301–5303.

(18) Korshavn, K. J., Jang, M., Kwak, Y. J., Kochi, A., Vertuani, S., Bhunia, A., Manfredini, S., Ramamoorthy, A., and Lim, M. H. (2015) Reactivity of metal-free and metal-associated amyloid- β with glycosylated polyphenols and their esterified derivatives. *Sci. Rep.* 5 (17842), 15.

(19) Hindo, S. S., Mancino, A. M., Braymer, J. J., Liu, Y., Vivekanandan, S., Ramamoorthy, A., and Lim, M. H. (2009) Small molecule modulators of copper-induced A β aggregation. *J. Am. Chem. Soc.* 131, 16663–16665.

(20) Hsu, F., Park, G., and Guo, Z. (2018) Key residues for the formation of A β 42 amyloid fibrils. *ACS Omega* 3, 8401–8407.

(21) Pederzoli, F., Ruozi, B., Duskey, J., Hagemeyer, S., Sauer, A. K., Grabrucker, S., Coelho, R., Oddone, N., Ottonelli, I., Daini, E., Zoli, M., Vandelli, M. A., Tosi, G., and Grabrucker, A. M. (2019) Nanomedicine against A β Aggregation by β -sheet breaker peptide delivery: In vitro evidence. *Pharmaceutics* 11, 572–602.

(22) Tjernberg, L. O., Naslund, J., Lindqvist, F., Johansson, J., Karlstrom, A. R., Thyberg, J., Terenius, L., and Nordstedt, C. (1996) Arrest of beta-amyloid fibril formation by a pentapeptide ligand. *J. Biol. Chem.* 271, 8545–8548.

(23) Ghanta, J., Shen, C.-L., Kiessling, L. L., and Murphy, R. M. (1996) A strategy for designing inhibitors of beta-amyloid toxicity. *J. Biol. Chem.* 271, 29525–29528.

(24) Lowe, T. L., Strzelec, A., Kiessling, L. L., and Murphy, R. M. (2001) Structure - function relationships for inhibitors of β -amyloid toxicity containing the recognition sequence KLVFF. *Biochemistry* 40, 7882–7889.

(25) Zhang, H., Dong, X., Liu, F., Zheng, J., and Sun, Y. (2018) Ac-LVFFARK-NH₂ conjugation to β -cyclodextrin exhibits significantly enhanced performance on inhibiting amyloid β -protein fibrillogenesis and cytotoxicity. *Biophys. Chem.* 235, 40–47.

(26) Chafekar, S. M., Malda, H., Merckx, M., Meijer, E. W., Viertl, D., Lashuel, H. A., Baas, F., and Scheper, W. (2007) Branched KLVFF tetramers strongly potentiate inhibition of β -amyloid aggregation. *ChemBioChem* 8, 1857–1864.

(27) Villari, V., Tosto, R., Di Natale, G., Sinopoli, A., Tomasello, M. F., Lazzaro, S., Micali, N., and Pappalardo, G. A. (2017) Metalloporphyrin-peptide conjugate as an effective inhibitor of amyloid- β peptide fibrillation and cytotoxicity. *ChemistrySelect* 2, 9122–9129.

(28) Lazzaro, S., Ogrinc, N., Lamont, L., Vecchio, G., Pappalardo, G., and Heeren, R. M. A. (2019) Ion mobility spectrometry combined with multivariate statistical analysis: Revealing the effects of a drug candidate for Alzheimer's disease on A β _{1–40} peptide early assembly. *Anal. Bioanal. Chem.* 411, 6353–6363.

(29) Zhang, G., Leibowitz, M. J., Sinko, P. J., and Stein, S. (2003) Multiple-peptide conjugates for binding β -amyloid plaques of Alzheimer's disease. *Bioconjugate Chem.* 14, 86–92.

(30) Ryan, P., Patel, B., Makwana, V., Jadhav, H. R., Kiefel, M., Davey, A., Reekie, T. A., Rudrawar, S., and Kassiou, M. (2018) Peptides, peptidomimetics, and carbohydrate-peptide conjugates as amyloidogenic aggregation inhibitors for Alzheimer's disease. *ACS Chem. Neurosci.* 9, 1530–1551.

(31) Tesaro, D., Accardo, A., Diaferia, C., Milano, V., Guillon, J., Ronga, L., and Rossi, F. (2019) Peptide-based drug-delivery systems in biotechnological applications: Recent advances and perspectives. *Molecules* 24, 351.

(32) Neri, P., Sessler, J. L., and Wang, M.-X. (2016) *Calixarenes and Beyond*, Springer International Publishing, Switzerland.

(33) Pan, Y.-C., Hu, X.-Y., and Guo, D.-S. (2021) Biomedical application of calixarenes: State of art and perspectives. *Angew. Chem., Int. Ed.* 60, 2768–2794.

(34) Viola, S., Consoli, G. M. L., Merlo, S., Drago, F., Sortino, M. A., and Geraci, C. (2008) Inhibition of rat glioma cell migration and proliferation by a calix[8]arene scaffold exposing multiple GlcNAc and ureido functionalities. *J. Neurochem.* 107, 1047–1055.

(35) Consoli, G. M. L., Granata, G., Picciotto, R., Blanco, A. R., Geraci, C., Marino, A., and Nostro, A. (2018) Design, Synthesis and antibacterial evaluation of a polycationic calix[4]arene derivative alone and in combination with antibiotics. *MedChemComm* 9, 160–164.

(36) Geraci, C., Consoli, G. M. L., Granata, G., Galante, E., Palmigiano, A., Pappalardo, M., Di Puma, S. D., and Spadaro, A. (2013) First self-adjutant multicomponent potential vaccine candidates by tethering of four or eight Muc1 antigenic immunodominant PDTRP units on a calixarene platform: Synthesis and biological evaluation. *Bioconjugate Chem.* 24, 1710–1720.

(37) Consoli, G. M. L., Granata, G., Fragassi, G., Grossi, M., Sallase, M., and Geraci, C. (2015) Design and synthesis of a multivalent fluorescent folate-calix[4]arene conjugate: Cancer cell penetration and intracellular localization. *Org. Biomol. Chem.* 13, 3298–3307.

(38) Granata, G., Paterniti, I., Geraci, C., Cunsolo, F., Esposito, E., Cordaro, M., Blanco, A. R., Cuzzocrea, S., and Consoli, G. M. L. (2017) Potential eye drop based on a calix[4]arene nanoassembly for curcumin delivery: Enhanced drug solubility, stability, and anti-inflammatory effect. *Mol. Pharmaceutics* 14, 1610–1622.

(39) Rodik, R. V., Anthony, A. S., Kalchenko, V. I., Mély, Y., and Klymchenko, A. S. (2015) Cationic amphiphilic calixarenes to compact DNA into small nanoparticles for gene delivery. *New J. Chem.* 39, 1654–1664.

(40) Zadnarm, R., and Alavijeh, N. S. (2014) Protein surface recognition by calixarenes. *RSC Adv.* 4, 41529–41542.

(41) Alex, J. M., Rennie, M. L., Engilberge, S., Lehoczki, G., Dorotyya, H., Fizil, Á., Batta, G., and Crowley, P. B. (2019) Calixarene-mediated assembly of a small antifungal protein. *IUCr* 6, 238–247.

(42) Wang, Z., Tao, S., Dong, X., and Sun, Y. (2017) Para-sulfonatocalix[n]arenes inhibit amyloid β -peptide fibrillation and reduce amyloid cytotoxicity. *Chem. - Asian J.* 12, 341–346.

(43) Xu, Z., Jia, S., Wang, W., Yuan, Z., Ravoo, B. J., and Guo, D. S. (2019) Heteromultivalent peptide recognition byco-assembly of cyclodextrin and calixarene amphiphiles enables inhibition of amyloid fibrillation. *Nat. Chem.* 11, 86–93.

(44) Geraci, C., Consoli, G. M. L., Galante, E., Bousquet, E., Pappalardo, M., and Spadaro, A. (2008) Calix[4]arene decorated with four Tn antigen glycomimetic units and P₃CS immunoadjuvant: Synthesis, characterization, and anticancer immunological evaluation. *Bioconjugate Chem.* 19, 751–758.

(45) Collins, J. M., and Leadbeater, N. E. (2007) Microwave energy: a versatile tool for the biosciences. *Org. Biomol. Chem.* 5, 1141–1150.

(46) Hilbich, C., Kisters-Woike, B., Reed, J., Masters, C. L., and Beyreuther, K. (1991) Aggregation and secondary structure of synthetic amyloid beta A4 peptides of Alzheimer's disease. *J. Mol. Biol.* 218, 149–163.

(47) Fasman, G. D. (1996) *Circular dichroism and the conformational analysis of biomolecules*, Plenum Press, New York.

(48) Sreerama, N., and Woody, R. W. (2000) Estimation of protein secondary structure from circular dichroism spectra: Comparison of CONTIN, SELCON, and CDSSTR Methods with an expanded reference Set. *Anal. Biochem.* 287, 252–260.

(49) Levine, H. (1993) Thioflavine T interaction with synthetic Alzheimer's disease β -amyloid peptides: Detection of amyloid aggregation in solution. *Protein Sci.* 2, 404–410.

(50) Yu, M., Ryan, T. M., Ellis, S., Bush, A. I., Triccas, J. A., Rutledge, P. J., and Todd, M. H. (2014) Neuroprotective peptide-

macrocycle conjugates reveal complex structure-activity relationships in their interactions with amyloid β . *Metalomics* 6, 1931–1940.

(51) Lomakin, A., Benedek, G. B., and Teplow, D. B. (1999) Monitoring protein assembly using quasielastic light scattering spectroscopy. *Methods Enzymol.* 309, 429–459.

(52) Morand, K., Talbo, G., and Mann, M. (1993) Oxidation of peptides during electrospray ionization. *Rapid Commun. Mass Spectrom.* 7, 738–743.

(53) De Bona, P., Giuffrida, M. L., Caraci, F., Copani, A., Pignataro, B., Attanasio, F., Cataldo, S., Pappalardo, G., and Rizzarelli, E. (2009) Design and synthesis of new trehalose-conjugated pentapeptides as inhibitors of $A\beta(1-42)$ fibrillogenesis and toxicity. *J. Pept. Sci.* 15, 220–228.

(54) Lambert, M. P., Barlow, A. K., Chromy, B. A., Edwards, C., Freed, R., Liosatos, M., Morgan, T. E., Rozovsky, I., Trommer, B., Viola, K. L., Wals, P., Zhang, C., Finch, C. E., Krafft, G. A., and Klein, W. L. (1998) Diffusible, nonfibrillar ligands derived from $A\beta(1-42)$ are potent central nervous system neurotoxins. *Proc. Natl. Acad. Sci. U. S. A.* 95, 6448–6453.

(55) Giuffrida, M. L., Tomasello, M. F., Pandini, G., Caraci, F., Battaglia, G., Busceti, C., Di Pietro, P., Pappalardo, G., Attanasio, F., Chiechio, S., Bagnoli, S., Nacmias, B., Sorbi, S., Vigneri, R., Rizzarelli, E., Nicoletti, F., and Copani, A. (2015) Monomeric α -amyloid interacts with type-1 insulin-like growth factor receptors to provide energy supply to neurons. *Front. Cell. Neurosci.* 9 (297), 16.